DOSE CHARACTERIZATION OF THE RAD SOURCE 2400 X-RAY IRRADIATOR

A Thesis

by

JENNIFER KOOP WAGNER

Submitted to the Office of Graduate Studies of
Texas A&M University
in partial fulfillment of the requirements for the degree of

MASTER OF SCIENCE

August 2008

Major Subject: Health Physics

DOSE CHARACTERIZATION OF THE RAD SOURCE 2400 X-RAY IRRADIATOR

A Thesis

by

JENNIFER KOOP WAGNER

Submitted to the Office of Graduate Studies of
Texas A&M University
in partial fulfillment of the requirements for the degree of

MASTER OF SCIENCE

Approved by:

Chair of Committee,	John Ford
Committee Members,	Eugene Blythe
	Leslie A. Braby
	Keith Maggert
	John W. Poston, Sr.
Head of Department,	Raymond Juzaitis

August 2008

Major Subject: Health Physics

ABSTRACT

Dose Characterization of the Rad Source 2400 X-Ray Irradiator. (August 2008)

Jennifer Koop Wagner, B.S., Texas A&M University

Chair of Advisory Committee: Dr. John Ford

The RS 2400 irradiator has been looked to as a replacement for discontinued gamma irradiators. The RS 2400 has a cylindrical, rather than point, x-ray source, which yields higher dose rates. The irradiator unit allows the user to set the current, voltage, and time for which the sample is to be irradiated, but gives no conversion between these values and the dose delivered. Working with Mississippi State University's Experimental Seafood Processing Laboratory (ESPL), the purpose of this research was to characterize the dose delivered by the RS 2400 for typical operating conditions.

The RS 2400 exposure rate increases, as expected, as the current and voltage are increased. The x-ray beam is uniform within 10% at the surface of the x-ray tube over a wide range of voltages, with the exception of the leftmost 5 cm of the tube, where structural supports are located. At the maximum operating parameters (150 kV and 45 mA), the beam has a first half value layer (HVL_1) of 13.66 mm aluminum, a homogeneity coefficient of 0.47, and equivalent photon energy ($h\nu_{eq}$) of 88.5 keV. This suggests a broad energy x-ray beam.

The maximum deliverable dose rate to tissue at the surface of the x-ray tube is 65 Gy min^{-1} ± 3.1%, but it is unlikely that any sample will ever be irradiated this close to

the x-ray tube. The standard sample canisters are 7.62 cm in diameter and the maximum deliverable dose rate to tissue at the canister location (with no canister present) is 37 Gy min^{-1} ± 3.1%. This is similar to the 45 Gy min^{-1} value that Rad Source Technologies, Inc. gives for the irradiator.

Irradiation of live oysters is of primary interest to the ESPL. For irradiation, oysters will most likely be placed in the 10.2 cm diameter plastic canisters since the 7.62 cm diameter canisters are not wide enough to hold larger oysters. The oyster shells and increased distance from the x-ray source reduce the maximum deliverable dose rate to 14.1 Gy min^{-1} ± 6.5% for thin-shelled oysters and 12.3 Gy min^{-1} ± 6.2% for thick-shelled oysters.

This work is dedicated to my family:

to my parents, who listen and support me in this and every project,

to my sister, who understands it and me,

and to Luke, the love of my life, who loves that I love cool science.

ACKNOWLEDGEMENTS

I would like to thank my committee chair, Dr. Ford, for his guidance and support as I pursued and carried out this research. My thanks also go to the staff at the Mississippi State University Experimental Seafood Reprocessing Laboratory, who allowed me to perform this research, and especially Jeff Dillion, who spent days helping me set up the experiment. Thanks also to Rad Source Technologies for answering questions about their irradiator. I am grateful to Dr. Poston, Dr. Braby, Dr. Maggert, and Dr. Blythe for providing feedback and for serving on my committee.

Thanks to the National Science Foundation's GK-12 program for providing me an assistantship that allowed me to pay my bills while I did this research. The students at Snook Middle School brightened my weeks and gave me a fresh perspective on the gift of education.

I have great appreciation and respect for the faculty and staff of the Nuclear Engineering Department and am happy to have been part of a wonderful department while I earned both of my degrees. Finally, thanks to the friends and roommates for such wonderful memories of graduate school.

NOMENCLATURE

ESPL	Mississippi State University's Experimental Seafood Processing Laboratory in Pascagoula, MS
SIT	Sterile Insect Technique
RS 2400	x-ray irradiator manufactured by Rad Source Technologies, Inc.
kV	kilovolt, measure of electrical potential
mA	milliampere, measure of current
cm	centimeter, unit of length
Z	atomic number, equal to the number of protons in an atom
E	energy
T	kinetic energy
T_0	initial kinetic energy
hv	photon energy
NSC	Nuclear Science Center at Texas A&M University
FIC	Nuclear Enterprises' 2571 0.6 cm^3 Farmer-type Ion Chamber
R	roentgen, unit of exposure
Gy	gray, SI unit of absorbed dose
Sv	sievert, SI unit of dose equivalent
rad	unit of absorbed dose equal to 0.01 Gy
rem	unit of dose equivalent equal to 0.01 Sv

TABLE OF CONTENTS

CHAPTER Page

LIST OF FIGURES

LIST OF TABLES

CHAPTER I

INTRODUCTION: MOTIVATION FOR THIS RESEARCH

When MDS Nordion quit manufacturing and maintaining their Gammacell™ 220 cobalt-60 irradiators, several laboratories looked to Rad Source Technologies to fill their needs with x-ray irradiators (Hendrichs 2007; Dinwiddie et al. 2000). X rays were used in biological irradiation experiments for decades, but use of gamma irradiators became increasingly more common due to their ability to deliver higher dose rates (Robinson 2005; Rugh and Wolff 1956). However, there are many economic and safety benefits associated with using non-radionuclide irradiators. Because the x rays are lower in energy than the gamma rays from cobalt-60, x-ray irradiators require far less shielding. This makes them lighter weight than comparable dose rate radionuclide irradiators and, therefore, much less expensive to ship. The expected cost for transport of a non-radionuclide irradiator from the U.S. to Europe is approximately $5,000 USD, one-tenth of the cost of transport of a radionuclide irradiator (Hendrichs 2007). X-ray irradiators also save time and money by avoiding paperwork and license requirements for radionuclide shipping, which can be costly and time consuming to acquire, particularly when shipping internationally (U.S. NRC 2007a). Finally, non-radionuclide irradiators eliminate the burden of radioactive material control and

---

This thesis follows the style of Health Physics.

accountability and reduce the probability that a source could be stolen, orphaned, used in a radiological dispersal device or cause radiation exposure accidents (Krippl 1996). This is particularly important in light of the fact that laboratories in developing countries without a strong nuclear regulatory body may wish to acquire irradiators. Sterile Insect Technique (SIT) laboratories, for example, have irradiated tsetse flies on Africa's Zanzibar Island and Mediterranean Fruit Flies in Argentina, Chile, Costa Rica, Guatemala, Peru, Mexico, and the Middle East (Johnston 2007).

The Entomology Unit of the Joint Food and Agriculture Organization (FAO)/International Atomic Energy Agency (IAEA) Program of Nuclear Techniques in Food and Agriculture purchased the RS 2500 x-ray irradiator and Mississippi State University's Experimental Seafood Processing Laboratory (ESPL) purchased the very similar RS 2400 x-ray irradiator. Both laboratories previously used Gammacell™ irradiators in their research. The FAO/IAEA Laboratory in Seibersdorf, Austria plans to use the irradiator as part of their SIT research and development projects. The SIT is a pest-control system in which male insects (primarily tsestse and Mediterranean fruit flies, as well as mosquitoes) are radiosterilized before being released in large numbers to mate with native females, resulting in a reduced pest population in the following generation. The ESPL intends to irradiate gulf coast oysters in an attempt to kill the *Vibrio vulnificus* and *Vibrio parahaemolyticus* bacteria that live on the oysters without damaging the oysters themselves. *Vibrio* bacteria are the cause of most food poisoning cases from eating raw oysters, but all other processing techniques currently available (steaming, pressurizing, and freezing) kill the oyster, which can affect the taste and

reduce the post-processing shelf-life. Mississippi State University may expand use of the irradiator to other areas, including induction of genetic mutations in plants.

The ESPL received its irradiator, the first of its kind, in the summer of 2007. The technical proposal for the irradiator states that it can deliver up to 45 Gy per minute, but the location of this measurement and whether it is dose to air or tissue is not given. The machine is able to deliver such high dose rates by using an extended anode design in which x rays are generated from a cylindrical surface rather than a point source (Rad Source Technologies 2007a). Upon delivery and installation, the irradiator does not have a dosimeter or any kind of conversion chart from current and voltage to dose rate. Before using the irradiator for research applications, the laboratories must either purchase and install a dosimeter of some kind or perform a dose characterization so that they know the dose that they are delivering to their samples. While installing a dosimeter would give the laboratories a reliable measure of dose delivered each time the irradiator is used, the dosimeters are expensive. Mississippi State University agreed to perform a dose characterization on their irradiator as the focus of this research and plans to use the results to determine the dose delivered in their experiments, at least for the time being.

Previous Work

With the cancellation of some Gammacell™ designs and the U.S. Nuclear Regulatory Commission encouraging alternatives to radionuclide sources and requiring time-intensive material control of such sources, the new high-dose rate Rad Source x-

ray irradiators may come into widespread use (Federline 2006). X-ray irradiators are currently being used for blood irradiation in North America (with between 50 and 100 units successfully operating at hospitals and medical institutes) (Mehta 2007). A blood irradiation center in Washington State has reported that the RS 3000 is a suitable alternative to the Gammacell^{TM} 3000 irradiator (Dinwiddie et al. 2000). Rad Source x-ray irradiators are currently used in the SIT project in the Republic of Panama (Hendrichs 2007).

The ESPL has done previous work using gamma radiation to inactivate *Vibrio* on oysters and other meats (Hu et al. 2005; Robertson et al. 2006). A Brazilian laboratory found that a dose of 1.0 kGy provided a 5 to 6 $\log_{10}$ reduction in *Vibrio* and *Salmonella*, meaning that the bacteria were reduced by 99.999% to 99.9999%. The highest dose delivered, 3.0 kGy, still allowed for oyster survival with no change to their odor, flavor, or appearance (Jakabi et al. 2002).

Thesis Research

At the ESPL, an active Farmer-type ion chamber was used to characterize the exposure rate within the exposure chamber. The exposure rate was measured at various currents and voltages, at various points along the canister length, inside canisters of various materials (plastic, cardboard, and aluminum), and inside thin and thick oyster shells. At the expected operating current and voltage, the x-ray beam was further characterized by determining the half-value layers using aluminum and copper. This

data was used to create a chart that translates current and voltage to dose rate delivered in the sample canister and to shelled oysters.

A more precise method of knowing the dose delivered to the oysters would be to place a disc ion chamber at the surface of the x-ray source and experimentally determine the conversion between the events detected by the ion chamber and dose delivered to the sample. This would correct for any problems caused if the x-ray generator operates for a slightly different time than the timer is set for and account for the fact that slightly more or less x rays will be produced as the machine breaks itself in by destroying impurities in the x-ray emitting target material. Unfortunately, the laboratory does not currently have the funding to purchase an ion chamber and building one is outside the scope of this research. The dose rate conversion allows the laboratory to determine, within a calculated error, the dose they are delivering to the sample. This allows them to begin their research program.

CHAPTER II

BACKGROUND

The RS 2400 Irradiator

The RS 2400 is an industrial cabinet x-ray irradiator. The total dimensions of the cabinet are 160 cm (63 inches) wide by 78.7 cm (31 inches) deep by 76.2 cm (30 inches) high, and the dimensions of the lead-shielded exposure chamber are 91.4 cm (36 inches) by 60.0 cm (24 inches) by 63.5 cm (25 inches) high. The control electronics are housed outside of the exposure chamber. Inside the exposure chamber is the cylindrical x-ray source and carousel system for holding the sample canisters. The carousel system holds 20.3 cm (8 inch) long canisters and has the option of rotating them around the x-ray source. The rotation option should be turned on during sample irradiation to ensure even exposure to all samples. The canister holders are hinged supports that are designed to hold 7.62 cm (3 inch) diameter canisters, but allow for some variance in canister size and can hold up to at least 10.2 cm (4 inch) diameter canisters. Canister holders can be changed to allow for up to 17.8 cm (7 inch) diameter canisters.

The U.S. version of the irradiator requires 208-volt AC, three-phase, 50/60 Hz, 40 amp input, while the European version requires 400-volt AC, three-phase, 50 Hz, 40 amp input (the irradiator at the ESPL in Mississippi is the U.S. version, naturally). The operating range of the x-ray tube varies from 25 kV to 150 kV and 2 mA to 45 mA, both continuously adjustable. In order to protect the x-ray tube from damage due to

excessively high temperatures, an operating current upper limit is set for the operating voltage (Table 1) (Rad Source Technologies 2007b).

Table 1. Operating current upper limit at various voltages.

Operating voltage (kV)	% of maximum current allowed	Operating current upper limit (mA)
30	5%	2.25
40	8%	3.60
50	10%	4.50
60	15%	6.75
70	20%	9.00
80	25%	11.25
90	30%	13.50
100	35%	15.75
110	40%	18.00
120	45%	20.25
125	50%	22.50
130	55%	24.75
140	65%	29.25
145	70%	31.50
150	100%	45.00

The Operator Touch Panel Control Screen sits on top of the irradiator cabinet and allows for relatively easy use of the irradiator. The screen turns on when the irradiator power is turned on. The screen allows the user to set the operating time and parameters (manual mode) or select a preset program (automatic mode). While x rays are being generated, the screen displays the actual kV and mA and counts down the time remaining in the exposure. If any alarms are triggered, they are displayed on the control screen.

The user can preset up to four programs that dictate the time, voltage, and current at which the irradiator will operate. In experiments where a similar irradiation will be repeated many times, it is useful to use a preset program to save time, reduce the possibility of human error in programming, and make users with less training feel more comfortable operating the irradiator.

Safety and Security Features

A key is required to turn on the irradiator. The password must then be entered through the control screen. A pre-warn time (set by the user) gives an alert that x ray production will soon begin. Two red, flashing lights on top of the irradiator are lit while x rays are being generated.

Alarms that prohibit x-ray generation can be triggered for several reasons. If both of the red light bulbs are out, the machine will not operate (if only one bulb is out, "single light failure" will be displayed on the control screen but the machine will still operate). If the access door (a small side door to allow for access to x-ray tube) or loading door (on top of the irradiator) are not securely closed, the machine will not operate. To protect the x-ray tube, any problems with the power supply, coolant water supply[*], or x-ray tube vacuum will prevent operation.

---

[*] In very hot regions, this safety feature is useful. The outlet temperature of the coolant water must be kept less than 110° F. As the irradiator only raises the temperature of the coolant by 10° F to 20° F, city-supplied water is more than cool enough in most areas. The ESPL found that summer water temperatures from the tap could exceed 96° F, hot enough to keep them from operating the irradiator during the daytime for a few months of the year. (The lab thinks that the water lines run close to the surface under asphalt pavement.) In order to have the freedom to run the irradiator year-round, the ESPL is considering adding a cooling element to the water supply line.

The X-Ray Generating Tube

The x-ray tube itself consists of a tungsten filament running down the center of a 10.2 cm (4 inch) diameter stainless steel cylinder. This is housed within a larger 11.4 cm (4.5 inch) diameter stainless steel cylinder. Both stainless steel cylinders are 0.17 cm (0.065 inches) thick. A layer of gold, 12 μm thick, is plated inside the inner cylinder. Figure 1 shows a cross section of the x-ray tube (Rad Source Technologies 2007b).

As the tungsten filament is heated, electrons are released from the surface. At higher currents (measured in mA), more electrons leave the filament. An electric potential difference (measured in kV) is applied between the filament and the inner tube, attracting the electrons toward the inner tube. A vacuum is drawn between the filament and the inner tube so the electrons do not interact with gas molecules. (The RS 2400 has its own vacuum pump and power supply.) The electrons gather a kinetic energy, T_0, equal to the potential difference; the higher the potential difference, the more energy the electrons gather. When the electrons reach the gold target plated inside the inner tube, they interact with the gold atoms and emit photons called x rays in all directions. For the energies used in the RS 2400, approximately 1% of the energy carried by the electrons freed from the filament is converted into x rays (Johns and Cunningham 1983). The remaining 99% is converted to heat energy and is removed by the water flowing between the inner and outer stainless steel tubes.

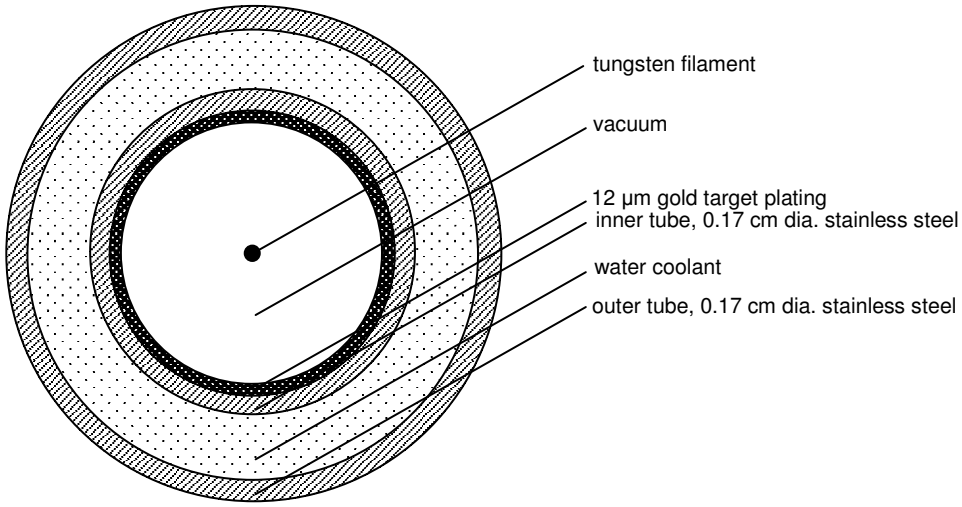

Fig. 1. Cross-section of x-ray tube (not to scale).

Interaction of Electrons with Target Atoms

Electrons freed from the filament interact with the target material via ionizing or radiative collisions. In ionizing collisions, the primary electron transfers energy to an electron bound to a target nucleus, kicking this secondary electron out of orbit. The primary electron may have many of these collisions before it loses all of its kinetic energy. The secondary electrons freed in these collisions are called delta rays.

If the primary electron kicks out a secondary electron in one of the inner electron shells, an electron from an outer shell can undergo a transition to fill the empty space and in doing so release a photon with energy *hv* equal to the difference in binding energies between the inner and outer shells. This is a radiative collision and the photons produced are called characteristic x rays or fluorescence x rays. These x rays are emitted isotropically. Quantum mechanic reasoning explains that transitions are more probable between certain energy levels and even forbidden between some energy levels.

Characteristic x rays resulting from freeing an election in the lowest energy shell, the *K*-shell, are most probable. For gold, the target material used in the RS 2400, the binding energy for *K*-shell electrons is 80.7 keV. Electrons with kinetic energy *T* less than the binding energy cannot transfer enough energy to free those electrons (Attix 2004). The K_α and L_α characteristic x rays are 68.8 keV and 9.7 keV, respectively (Feldman and Mayer 1986). The low energy L_α x ray is unlikely to be seen as it tends to be attenuated in cooling or support material before it reaches a detector or sample.

A second kind of radiative collision occurs if the electron interacts with the nucleus itself. As the electron closely approaches the nucleus, it changes direction and loses kinetic energy, which is emitted as electromagnetic radiation in the form of a photon. This is called bremsstrahlung radiation, German for "braking radiation". The probability that the electron will transfer all of its kinetic energy to a bremsstrahlung photon is small, but it is equally probable that any energy bremsstrahlung photon with energy $h\nu$ less than T_0 will be created. These photons are emitted in all directions, but anisotropically; they tend to be emitted in the direction of the electron path. Higher *Z* target materials (like gold, $Z = 79$) transfer a greater fraction of the electron's kinetic energy to bremsstrahlung x ray production than do lower *Z* materials. Figure 2 summarizes the ionizing and radiative interactions of electrons (Attix 2004; Johns and Cunningham 1983).

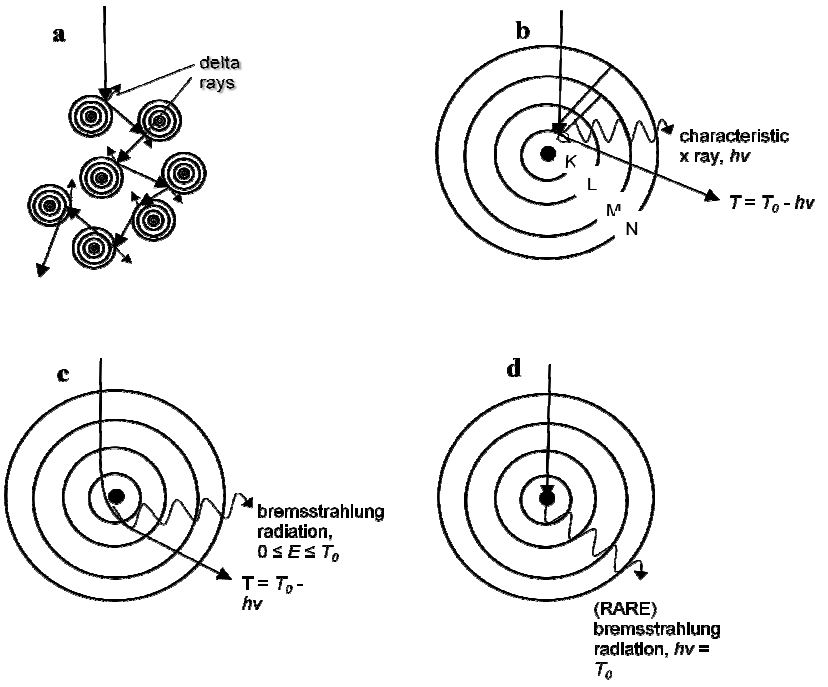

Fig. 2. Electron interactions with target atoms. The electron, with kinetic energy T_0, can interact via (a) ionization of secondary electrons called delta rays, (b) radiative production of characteristic x rays, (c) radiative production of bremsstrahlung photons, (d) rare interactions where electron converts its entire kinetic energy to bremsstrahlung photon.

X-Ray Energy Spectrum

Figure 3 gives a schematic of the photon energy spectrum for x rays produced in a gold target from interactions with electrons with T_0 = 150 keV. The grey boxes show the bremsstrahlung photon spectra for a thick target material, defined as any material thick enough that the electron will tend to have more than one interaction. The probability that the electron will transfer all of its energy directly, producing one bremsstrahlung photon, is small, but there is an equal probability that it will yield a bremsstrahlung photon of any energy greater than zero and less than T_0. The reduced energy electron remains available to give rise to another bremsstrahlung photon and so

on, giving a linear spectrum of photons. The characteristic x rays for gold are superimposed on this spectrum. The stainless steel tubes, cooling water, and any other material between the gold target and the detector (or sample) filter out the low energy photons from the x-ray beam. The beam energy typically peaks somewhere around 30 to 40 keV and very few photons with energy less than 20 keV make it through the filtration materials (Johns and Cunningham 1983).

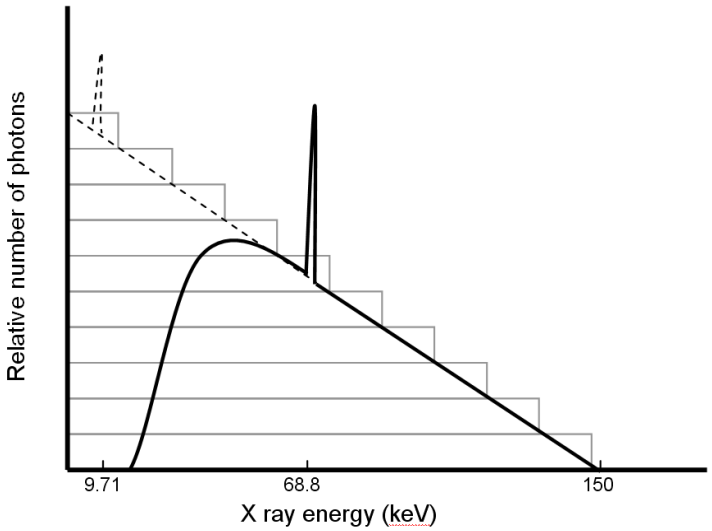

Fig. 3. Schematic energy spectrum for x rays produced in gold target from interactions with electrons with T_0 = 150 keV. The dotted line shows low energy photons that are filtered out by support and cooling materials surrounding the target.

Although the characteristic x rays make distinctive peaks in the graph, they are a relatively small percent of the total x-ray energy emitted; the bremsstrahlung photons account for most of the energy in the x-ray beam. In a completely unfiltered x-ray beam, if the number of electrons incident on the target is doubled (by increasing the

current), then the relative number of photons of each energy is doubled, and the total energy of the x-ray beam is doubled. If the kinetic energy of the electrons, T_0, is doubled, the total energy of the x-ray beam is approximately quadrupled. The x rays produced are now free to interact with and deposit energy in material in the ways any photon would: via the photoelectric effect, Compton scattering, and pair production. (X rays produced in the RS 2400 will never undergo pair production: at a maximum, their energy *hv* is 150 keV, well below the 1.022 MeV threshold for pair production.)

Error Calculation and Propagation

The equation used to calculate the experimental sample variance, s^2, for points at which multiple measurements were taken is:

$$s^2 = \frac{1}{N-1}\sum_{i=1}^{N}(x_i - \overline{x_e})^2 \tag{1}$$

where N is the number of number of measurements, x_i is the experimental value, and x_e is the experimental mean. This equation was used throughout the experiment. For all further calculations, the error was propagated using standard error propagation formulas. The general equation for error propagation for a quantity u derived from x, y, z, … is:

$$\sigma_u{}^2 = \left(\frac{\partial u}{\partial x}\right)^2 \sigma_x{}^2 + \left(\frac{\partial u}{\partial y}\right)^2 \sigma_y{}^2 + \left(\frac{\partial u}{\partial z}\right)^2 \sigma_z{}^2 + \ldots \tag{2}$$

where $\sigma_u{}^2$ is the variance in value u, $\sigma_x{}^2$ is the variance in value x, and so on. For addition or subtraction, such as in eqn (3), eqn (2) yields eqn (4)

$$u = x + y \text{ or } u = x - y \tag{3}$$

$$\sigma_u = \sqrt{\sigma_x{}^2 + \sigma_y{}^2}\,. \tag{4}$$

When multiplying or dividing by a constant, as in eqn (5), eqn (2) yields eqn (6)

$$u = Ax \text{ or } u = \frac{x}{B} \tag{5}$$

$$\sigma_u = A\sigma_x \text{ or } \sigma_u = \frac{\sigma_x}{B}\,. \tag{6}$$

Multiplying or dividing two values, such as in eqn (7), yields eqn (8) (Knoll 2000)

$$u = \frac{x}{y} \text{ or } u = xy \tag{7}$$

$$\left(\frac{\sigma_u}{u}\right)^2 = \left(\frac{\sigma_x}{x}\right)^2 + \left(\frac{\sigma_y}{y}\right)^2. \tag{8}$$

CHAPTER III

IRRADIATOR CHARACTERIZATION: EXPERIMENT AND RESULTS

Farmer-Type Ion Chambers

A Nuclear Enterprises 2571 Farmer-type ion chamber (Fig. 4) was used to measure the exposure in the RS 2400. The ion chamber thimble is 0.69 cm^3 and connects to the electronics box, which remains outside of the exposure chamber, via a triaxial cable. The walls of the thimble are made of 99.99% pure graphite and are 0.36-mm thick, with a 3.87-mm thick graphite build-up cap that can be added to maintain charged particle equilibrium for higher energy x-ray beams. The ion chamber specifications give the energy range of x rays from 50 kV to 300 kV without the build-up cap or 300 kV to 2 MV with the build-up cap (Nuclear Enterprises Limited 1980). To confirm that the build-up cap should not be used, a quick comparison of the exposure measured with and without the build-up cap was done with the RS 2400. At 150 kV and 45 mA, 12-second measurements taken on the surface of the x-ray tube were, on average, 947.6 ± 0.5 R without and 853.3 ± 0.9 R with the build-up cap. The first value is assumed to be correct; when the build-up cap is added, the thicker wall removes lower-energy, secondary-charged particles from the beam before they enter the sensitive volume, reducing the exposure. All characterization measurements were done without the build-up cap.

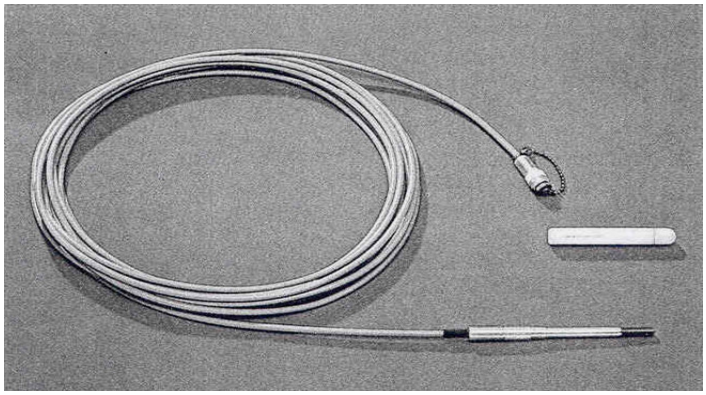

Fig. 4. Farmer-type ion chamber. Shown are the thimble, triaxial connective cable, and removable buildup cap (Nuclear Enterprises Limited 1980).

Calibration of the FICs

The Farmer-type ion chambers (FICs) were calibrated using the x-ray beam at Texas A&M University's Nuclear Science Center (NSC) (Texas A&M University NSC 2001). After completing training on how to operate the NSC x-ray chamber, FICs were calibrated by exposing them in the x-ray beam, comparing the values to the well-calibrated NSC FIC, and calculating the calibration factor as the ratio between the actual exposure (as measured by the NSC FIC) and the exposure measured on the new FIC. After warming up the x-ray tube as per instructions in the operating manual, preliminary calibrations were performed by taking ten exposure measurements at 250 kV and 10.0 mA. Initially, the FICs were placed on the lowest shelf of the x-ray chamber to ensure that both were within the x-ray beam, but the shelf was moved up to the center position for the last 5 measurements in order to reduce the exposure times. The preliminary calibration factor for FIC 1 was 0.99 ± 0.9%. While the experimental plan called for the

use of FIC 1, a second FIC was calibrated as a back-up. The preliminary calibration factor for FIC 2 was 1.33 ± 0.5%.

After taking measurements on the RS 2400, a more thorough calibration of FIC 2 was conducted to determine if the calibration factor was constant as the x-ray beam energy changed. Ten exposures were taken at 9.0 mA and T_0 beam energies between 100 kV and 150 kV. The calibration factor remained approximately constant across the energy range at 1.42 ± 2.8%. Exposure measurements and more detailed information on FIC calibration can be found in Appendix A.

Experimental Set-Up

To limit exposure outside of the chamber, there is no direct open path into the RS 2400. Samples to be irradiated are put into the chamber via a sliding door on the top of the irradiator, but, because the safety interlocks require that this door be firmly closed in order for the machine to operate, the cable could not be fed through this pathway. The only usable entry to the chamber was a labyrinth-like passage that opens underneath the chamber, approximately twelve inches from the floor of the laboratory. This labyrinth is effective at shielding the outside area from x-ray exposure, since radiation is scattered and attenuated by the turns.

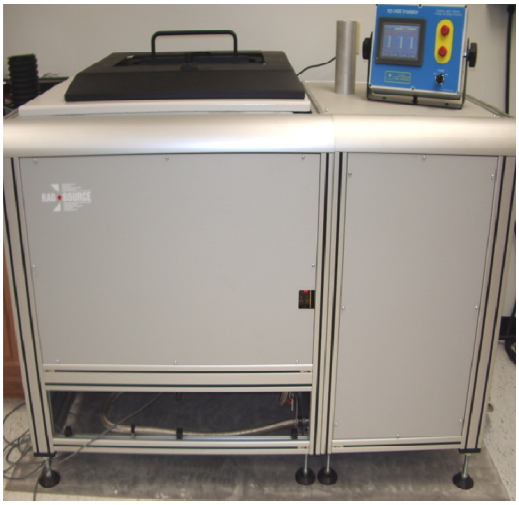

Fig 5. ESPL's RS 2400 irradiator (with lower front panel removed to allow detector input).

As shown in Fig. 5, the front and side panels of the machine were removed to allow more access to the labyrinth and, after many hours and attempts to use various styles of commercially-available and modified cable threaders, the ion chamber was guided into the exposure chamber by hand using two people. The first person (with the smaller arm) guided the cable from underneath the machine while the second stood above the exposure chamber to visualize and direct the cable and pull it into the exposure chamber. In the process of setting up the experiment, the triaxial cable on FIC 1 was damaged and FIC 2 had to be used.

To determine the affect of canister material on exposure, measurements were taken at the same position with and without the canister present. To hold the ion chamber in place, thin aluminum wire for the FIC to rest on was strung at the same distance from the x-ray tube surface as the center of the canister (Fig. 6). For the 7.62 cm (3 inch) diameter canisters, the center of the canister is 7.62 cm (3 inches) from the

tube surface. For 10.2 cm (4 inch) diameter canisters, the center of the canister is 8.9 cm (3.5 inches) from the tube surface. The FIC was always placed at the center of the canister because the canisters are set to rotate around the x-ray tube, so a sample placed anywhere in the canister will be separated from the tube surface, on average, the distance from the tube surface to the center of the canister. (The rotation mode was turned off while measurements were taken to avoid wrapping the triaxial cable around the x-ray tube.)

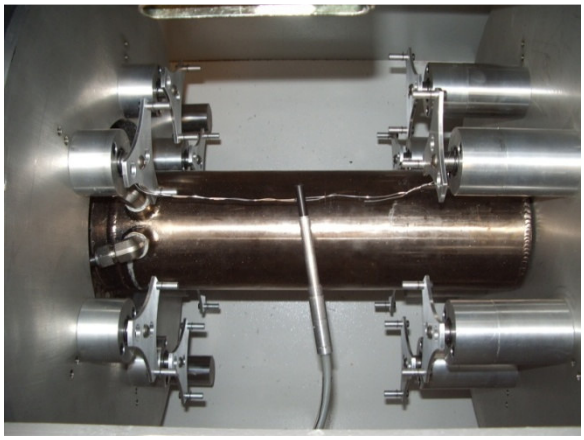

Fig. 6. Farmer-type ion chamber in RS 2400 exposure chamber. The FIC is resting on a thin aluminum wire. The x-ray tube (center) and canister holders can be seen.

Thin sheets of aluminum flashing and aluminum wire were to be used to act as springs to hold the FIC in the center of the canisters. The flashing is thin and aluminum has a relatively low atomic number, $Z = 13$, so it was expected to be virtually transparent to x rays (Winter 2008). A quick comparison of 20-second exposures with and without the aluminum flashing in the RS 2400 proved this to be incorrect. At a

position 7.62 cm (3 inches) from the surface of the tube and with operating parameters of 150 kV, 45 mA, the exposure without the flashing was 922 R ± 6% and with the flashing was 712 ± 0.3%. The flashing decreased the 20-second exposure by 23%. Aluminum flashing was not used to hold the FIC in place for any of the calibration measurements; instead, it was held by thin aluminum wire (Fig. 7).

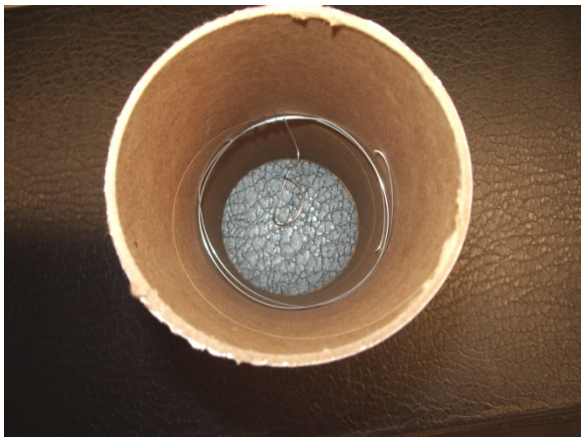

Fig. 7. Aluminum wire support in cardboard canister (7.63 cm diameter).

For the measurements taken in canisters, the FIC was aligned so that its axis was parallel to the axis of the x-ray tube to ensure that the entire sensitive volume was exposed to the same photon field. The FIC should have been aligned in the same way for measurements taken without canisters, but to balance the FIC on the aluminum wire, it was aligned them as shown in Fig. 6. This likely introduced additional error, but variations in the x-ray field across the FIC were likely to be small since the length of the FIC is much less than the diameter of the x-ray tube.

Exposure Rate Characterization

The exposure was measured, in roentgen, at various positions within the exposure chamber and at varying operating parameters. Ideally, several measurements would have been taken at each point, but with a limited time in which to complete the experiment and more time than expected taken up by set-up, multiple measurements were made only at the positions and parameters that the laboratory would routinely use for sample exposures. For example, while exposure measurements were made at the surface of the x-ray tube, it was not expected that a sample would ever be irradiated on the surface of the tube. Practically, the sample holders are several inches from the surface of the tube. In their previous irradiation work with a gamma source, the laboratory delivered up to 3 kGy to oysters (Andrews et al. 1998; Hu et al. 2005). Live oysters should not be allowed to remain at or above room temperature for any longer than necessary. Thus, it was assumed that the highest operating settings (150 kV and 45 mA) would be used to deliver the dose as quickly as possible. The canister used to hold the oysters needed to be both large enough to hold them and able to withstand any dripping water. The RS 2400 was delivered with two sets (six canisters per set) of 7.62 cm (3 inch) diameter canisters: one aluminum and one cardboard. Neither of these canisters was appropriate for oyster irradiation: while the aluminum canisters were water resistant, the diameter of the canisters was too small to hold larger oysters. Corrugated plastic tubing 10.2 cm (4 inches) in diameter was purchased from a hardware store and cut into set of canisters for oyster irradiation.

Exposure Rate as a Function of Linear Position

Exposure measurements were taken along the surface of the x-ray tube to determine if the exposure rate varied across the length of the tube. Facing the RS 2400 and looking down into the exposure chamber, positions were marked off every 2.54 cm (1 inch) from the left side. The maximum allowable anode current setting (Table 1) was used at each voltage setting. Two to three measurements, ranging from 8 seconds each at the highest voltage to 20 seconds at the lowest, were taken at each voltage setting: 60 kV, 120 kV, and 150 kV. The exposure time was varied with the aim of obtaining the largest exposure that would fit on the FIC readout to minimize the percent error in the measurement. Even using a magnifying lens, it was not possible to read the exposure dial with extreme precision, so all measurements have a reading uncertainty of ± 0.5 R in addition to the error in the data set. Measurements were multiplied by the calibration factor and converted to exposure rate (R min^{-1}). No measurements were noticeable outliers and no data points were excluded with Chauvenet's criterion (Kirkup 2002). The average was calculated and error propagation formulas (eqns (2) through (8)) were used to calculate the standard deviation (σ). This method was used to determine the average and error in all following calculations, as well.

The results, displayed in Fig. 8, show that the exposure rate is not constant across the length of the tube. The trend is constant over the three voltages tested: there is a slight increase in exposure rate at position 7 and a drastic decrease at positions 0 and 1. If these two positions (0 and 1) were excluded and the average for the other eight positions is determined, they are an average of 68% and 38% lower, respectively, than

the average exposure rate. All other data points are within 10% of the average exposure rate (Table 2). At the maximum operating parameters (150 kV and 45 mA), the exposure rates were, on average, within 3.1% of each other. The operations manual claims that the beam uniformity is ±3% at a 15.2 cm (6 inch) radius from the x-ray tube (Rad Source Technologies 2007b). This uncertainty should be added to any calculation of exposure rate to samples.

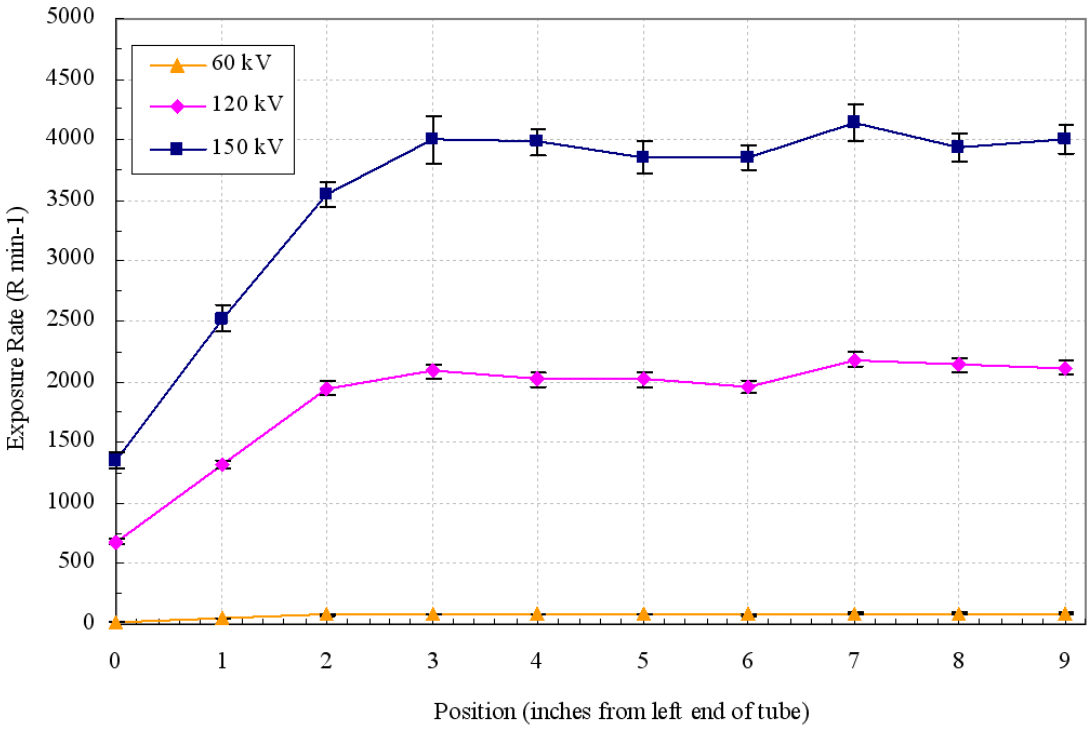

Fig. 8. Exposure rate along length of x-ray tube. The current is set at the maximum allowable mA for the voltage (see Table 1). All measurements were taken at the surface of the x-ray tube, at the center of the tube length. Error bars are ± $\sigma_{R\ min\text{-}1}$.

The manufacturer of the RS 2400 did not expect the exposure rate to be constant near the ends of the x-ray tube[†]. Structural supports on the left side of the tube significantly decreased the exposure rate. The implication of this is that samples should not be placed within 5 cm (2 inches) of the left of the x-ray tube. Sample canisters are only 20.3 cm (8 inches) long and centered along the tube length, so samples will not be placed within the first inch. If at all possible, the samples should be placed at least 2.54 cm (1 inch) from the left side of the canister.

Table 2. Exposure rate variance over length of x-ray tube.

kV	mA	Position (inches from left)	% difference in exposure rate from pos. 2-9 average
60	6.8	0	**72.99%**
		1	**42.37%**
		2	7.75%
		3	3.07%
		4	4.23%
		5	2.36%
		6	9.05%
		7	9.07%
		8	8.56%
		9	8.82%
120	20.3	0	**66.96%**
		1	**36.16%**
		2	5.39%
		3	1.41%
		4	1.92%
		5	1.80%
		6	4.98%
		7	6.03%
		8	3.88%
		9	2.76%
150	45	0	**65.53%**
		1	**35.58%**
		2	9.27%
		3	2.15%
		4	1.70%
		5	1.54%
		6	1.58%
		7	5.66%
		8	0.51%
		9	2.36%

[†] personal conversation with Phil Ausburn, Rad Source Technologies, August 2007

Exposure Rate as a Function of Current

Measurements of exposure as a function of current (mA) were taken at the center on the surface of the x-ray tube. Measurements were taken every 5 mA up to the maximum allowed current for the voltage. At all of the measured voltages (120 kV, 130 kV, 140 kV, and 150 kV), exposure rate increased approximately linearly (R^2 values range from 0.97 to 0.999), as expected (Fig. 9).

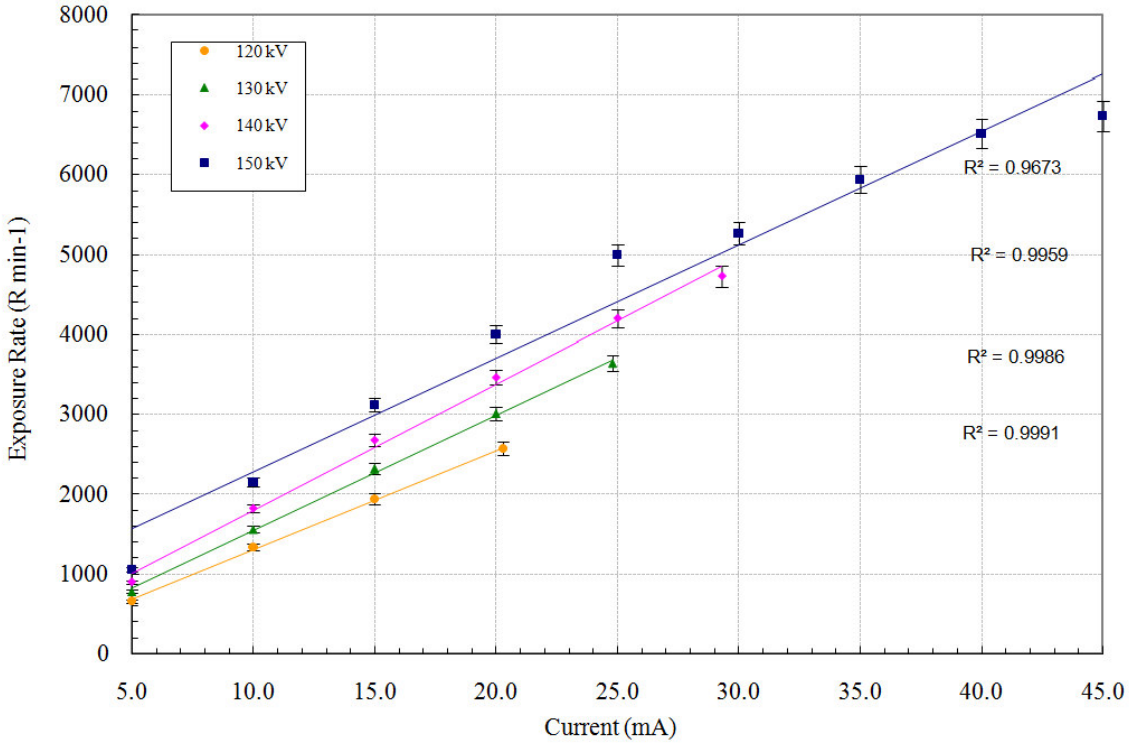

Fig. 9. Exposure rate as a function of current. All measurements were taken at the surface of the x-ray tube, at the center of the tube length. Error bars are ± $\sigma_{R\ min\text{-}1}$.

Effect of Canisters on Exposure Rate

Figure 10 shows the exposure rate as a function of voltage in sample canisters.

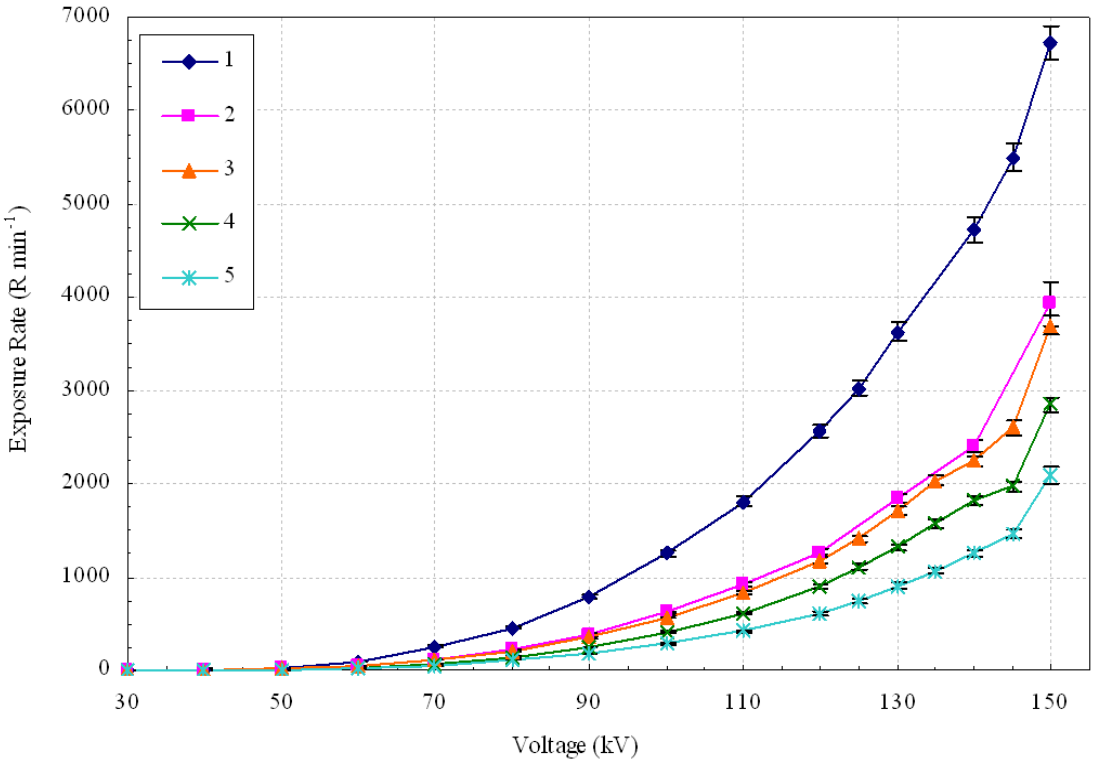

Fig. 10. Exposure rate in various sample canisters as a function of voltage. The current is set at the maximum allowable mA for the voltage (see Table 1). All measurements were taken at the center of the x-ray tube length, but the distance from the x-ray tube surface and canister material varied. (1) no canister, at x-ray tube surface, (2) no canister, located at center of 3" diameter canister, (3) cardboard canister (3" diameter), (4) aluminum canister (3" diameter), and (5) plastic canister (4" diameter). Error bars are ± $\sigma_{R\ min\text{-}1}$.

The voltage was stepped up from 30 kV, the minimum allowable, to the 150 kV maximum in 5 kV or 10 kV intervals. The maximum allowable current setting was used at each voltage setting, and all measurements were taken halfway between the left and right ends of the x-ray tube. The exposure times ranged from 8 seconds to 60 seconds.

Data series 1 measurements were taken at the surface of the x-ray tube with no canister, series 2 at the center position of the 7.62 cm (3 inch) diameter canister but with no canister present, series 3 at the center of the 7.62 cm (3 inch) diameter cardboard canister, series 4 at the center of the 7.62 cm (3 inch) diameter aluminum canister, and series 5 at the center of the 10.2 cm (4 inch) diameter plastic canister. Points at which multiple measurements were taken have larger error bars, but in some cases these are still too small to be seen on the graph.

Effect of Oyster Shells on Exposure Rate

The ESPL plans to use the RS 2400 to irradiate live oysters in shells that attenuate x rays and reduce the dose to the oyster tissue. Oyster shells come in a variety of sizes and thicknesses. To determine how much the shell reduced the exposure rate (and therefore dose rate) to the oyster tissue and how significant the shell thickness was, two oyster phantoms were fabricated (Fig. 11) by layering thick or thin shells over a plastic bag filled with water.

Fig 11. Oyster shells of various sizes and thicknesses (left) and an oyster phantom (right). The phantoms consisted of two oyster shells of similar thicknesses covering a plastic bag filled with water. The FIC was placed inside the phantom.

Figure 12 shows that, as expected, the thick oyster shells reduced exposure rate more than thin oyster shells. The percent difference in exposure rates between the thick and thin-shelled phantoms remained constant at about 15% ± 4.6%, but the percent decrease from no shell varied with the applied voltage (Table 3). The exposure rate was similar for unshelled, thin-shelled, and thick-shelled oysters until the voltage exceeded 130 kV.

Table 3. Effect of oyster shells on exposure rate.

kV	Thick oyster shell % difference from no shell	Thin oyster shell % difference from no shell	% difference between thick and thin oyster shells
100	-6.32% ± 4.0%	6.41% ± 4.1%	13.60%± 4.5%
110	-5.84% ± 4.1%	8.58% ± 4.4%	15.31% ± 4.3%
120	-9.74% ± 4.0%	5.10% ± 4.4%	16.45% ± 4.9%
130	-12.16% ± 3.7%	2.19% ± 4.0%	16.33% ± 4.3%
140	-25.67% ± 3.6%	-13.70% ± 3.7%	16.10% ± 4.3%
150	-38.17% ± 4.8%	-29.22% ± 4.9%	14.47% ± 5.0%
		Avg % diff=	15.38% ± 4.6%

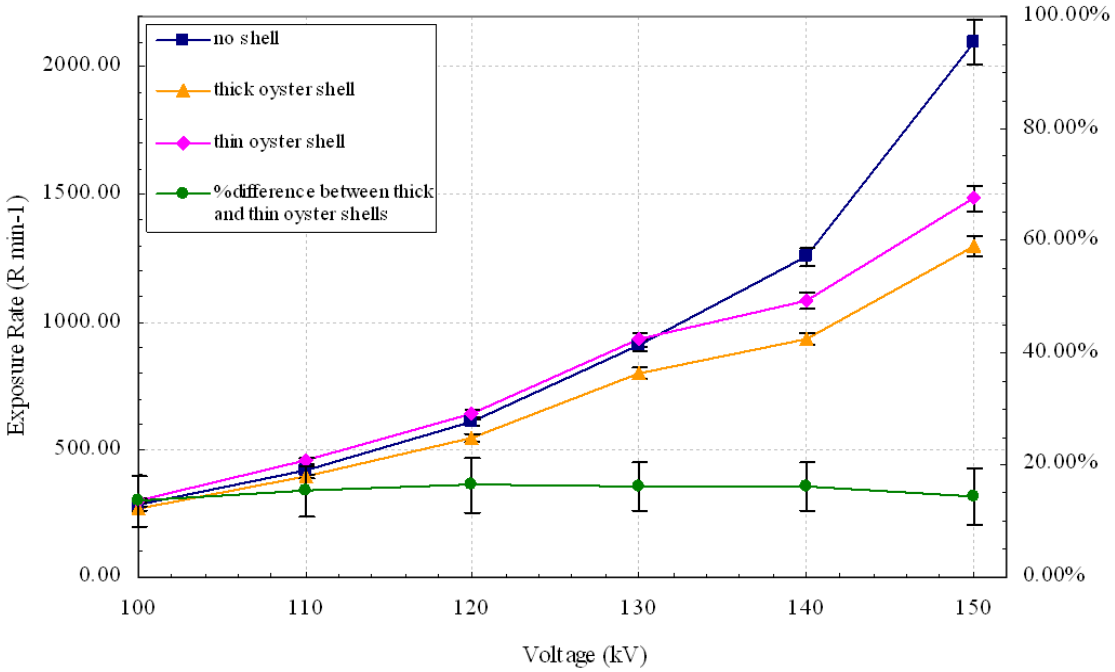

Fig. 12. Reduction in exposure rate by oyster shells. The exposure rate for no shell, thin shell, and thick shell phantom oysters is given on the left axis. The % difference between thick and thin shells is given on the right axis. Error bars are ± $\sigma_{R\ min\text{-}1}$.

X-Ray Beam Characterization

To deliver the desired dose while minimizing exposure time, it was expected that the RS 2400 would most often be operated at 150 kV and 45 mA. To characterize this x-ray beam, thin metal attenuator sheets were used to determine the half-value layer, *HVL*, defined as the thickness necessary to reduce the exposure by half in narrow-beam geometry. Narrow-beam geometry requires that no scattered x rays reach the detector; only those photons coming through the attenuator (aluminum or copper) should be counted. It is more difficult to meet this requirement with a cylinder source than with a point source, but by using attenuator sheets that were much larger than the FIC and completely covering it, this was condition was approximated (though some amount of

photon inscatter likely still occurred). Both aluminum and copper were used; aluminum is preferred for lower-energy x-ray beams (T_0 less than or equal to approximately 120 keV) while copper is preferred for higher-energy x-ray beams (T_0 up to 500 keV). The aluminum values more accurately characterized this beam, $T_0 = 150$ keV. The final convention for calculating *HVL* requires that the detector be air-equivalent and give a constant response per unit exposure, independent of photon energy, which is satisfied by the FIC (Attix 2004).

To ensure that the position of the detector did not change during the *HVL* measurements, a spot was marked on the floor of the exposure chamber, directly underneath and 33.7 cm (13.25 inches) below the center of the x-ray tube. Five 20-second measurements were taken without any attenuator and the average FIC reading was determined to be 183.24 R ± 1.3%. (None of the *HVL* measured exposures by the conversion factor to determine the actual exposure since the conversion factor was constant across x-ray energies and doing so would introduce additional error.) Attenuator layers were added until the 20-second exposure was reduced to half and one-quarter of the original value. The thickness at which the exposure was reduced by half is the first *HVL*, HVL_1. The thickness at which that value is again reduced by half (or the original, unattenuated value is reduced to one-quarter) is the second *HVL*, HVL_2. The ratio of the first to the second half-value layers is the homogeneity coefficient, *HC:*

$$HC = \frac{HVL_1}{HVL_2} . \tag{9}$$

The *HC* describes how broad or narrow the energy spectrum of the beam is; *HC* is equal to unity for a perfectly monoenergetic beam and decreases (but always remains greater than zero) for broader energy range beams.

HVL_1 can also be used to determine the equivalent photon energy of the x-ray beam, hv_{eq}, which is defined as the energy of a monoenergetic beam that would have the same HVL_1 as the x-ray beam being characterized. This relationship is described by the following equation:

$$\frac{X}{X_0} = 0.5 = e^{-(\mu/\rho)_{eq} \times HVL_1 \times \rho} \tag{10}$$

which can be rearranged as:

$$\left(\frac{\mu}{\rho}\right)_{eq} = \frac{0.6931}{\rho \times HVL_1} cm^2 / g \tag{11}$$

where X is the exposure, ρ is the density of the attenuator, and $(\mu/\rho)_{eq}$ is the mass attenuation coefficient for hv_{eq} in the material used as an attenuator. The densities of naturally abundant aluminum and copper are 2.7 g cm^{-3} and 8.9 g cm^{-3}, respectively (Engineers Edge 2008). By determining the (μ/ρ) values and the corresponding photon energies in a table and interpolating, one can solve for hv_{eq} (Attix 2004).

Figure 13 shows the relative exposure (20-second exposure at attenuator thickness divided by 20-second exposure without attenuator) for increasing attenuator thicknesses. An exponential trend line was fit to the data. Broad curves, like these, indicate a broad spread in x-ray beam energies, while a more linear curve would

indicate an x-ray beam that is closer to monoenergetic. *HVLs*, *HC*, $(\mu/\rho)_{eq}$, and hv_{eq} for aluminum and copper are shown in Table 4.

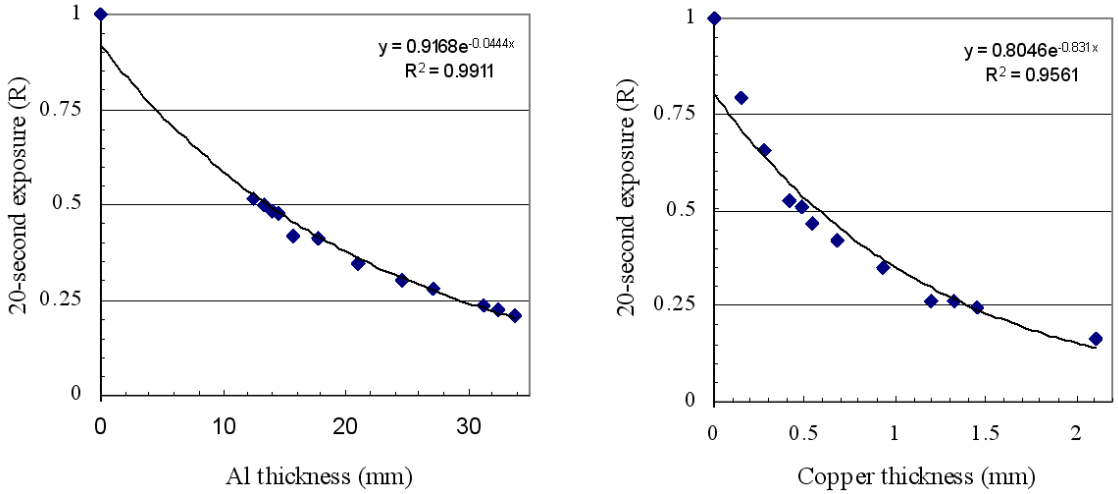

Fig. 13. Relative exposure as a function of attenuator thickness (150 kV, 45 mA x-ray beam). This data was used to determine the half-value layers of aluminum and copper.

The copper attenuator gave lower *HC* and hv_{eq} values than aluminum: about 13% lower HC and 26% lower hv_{eq}. The aluminum values were used for any further calculations.

Table 4. X-ray beam characterization using aluminum and copper attenuators.

Aluminum attenuator					Copper attenuator				
HVL₁ (mm)	***HVL₂*** (mm)	***HC***	$(\mu/\rho)_{eq}$ (cm^2/g)	hv_{eq} (keV)	HVL_1 (mm)	HVL_2 (mm)	*HC*	$(\mu/\rho)_{eq}$ (cm^2/g)	hv_{eq} (keV)
13.66	**29.27**	**0.47**	**0.1879**	**88.45**	0.5725	1.407	0.41	1.360	65.77
		% difference from Al values:					- 12.77%		- 25.64%

Converting Exposure to Dose

Under conditions of charged particle equilibrium, the exposure, X, is related to the absorbed dose in air, D_{air}, as shown in eqn (12) (units are given in square brackets)

$$D_{air}\left[\frac{J}{kg}\right] \overset{CPE}{=} X\left[\frac{C}{kg}\right]\times\left(\frac{\overline{W}}{e}\right)_{air}\left[\frac{J}{C}\right] = 8.764\times10^{-3}\times X\left[R\right] \tag{12}$$

where $(W/e)_{air}$ is 33.97 joules per coulomb for dry air (Attix 2004).

The dose delivered depends on the composition of the material to which it is being delivered. The ESPL is interested in irradiating oysters, which are entirely soft tissue. Air has a similar atomic composition to soft tissue and therefore a similar effective atomic number, Z_{eff}. This means that radiation will interact with it in a similar way and makes it a suitable tissue-equivalent material. Water is an even better tissue-equivalent because its Z_{eff} is closer to that of soft tissue (Table 5) (Jayachandran 1971; Bomford et al. 2002).

Table 5. Z_{eff} for tissue and tissue-equivalent materials.

Material	Z_{eff}
air	7.64
water	7.42
soft tissue	7.35[a] to 7.36[b]

[a] Bomford 2002, [b] Jayachandran 1971

Under conditions of CPE, the ratio of the absorbed dose in material A, D_A, to the absorbed dose in material B, D_B, is equal to the ratio of their energy absorption coefficients, μ_{en}/ρ (Attix 2004)

$$\frac{D_A}{D_B} \overset{CPE}{=} \frac{\left(\mu_{en}/\rho\right)_A}{\left(\mu_{en}/\rho\right)_B} . \tag{13}$$

Mass attenuation coefficient tables were available for air and water, but not soft tissue, so dose rate in water was used as an approximation for dose rate in tissue. At the maximum machine operating parameters (150 kV and 45 mA set points), where hv_{eq} = 88.45 keV, the absorbed dose rate in tissue is related to the absorbed dose rate in air by eqn (14)

$$\dot{D}_{tissue} \approx 1.084 \times \dot{D}_{air} . \tag{14}$$

The quality factor, Q, for x rays is defined as 1. Therefore, the value of absorbed dose (in Gy or rad) is equal to the value of equivalent dose (in Sv or rem) (U.S. NRC 2007b). Table 6 gives exposure and dose rates at various voltages (and the maximum allowable current settings for the voltage) for shelled and unshelled tissue. Tables in Appendix D give exposure and dose rates to tissue for 7.62 (3 inch) diameter cardboard and aluminum canisters, which may be useful for irradiating other kinds of samples.

The maximum deliverable absorbed dose rate to tissue in the 10.2 cm (4 inch) diameter corrugated plastic canister with no oyster shell was approximately 20 Gy min^{-1} ± 4.1% (including the uncertainty from beam non-uniformity). This is considerably less than the 45 Gy min^{-1} that Rad Source Technologies claims that the RS 2400 delivers

(Rad Source Technologies, Inc. 2007b). As previously discussed, there was no position associated with this given dose rate. At the surface of the x-ray tube with no canister, a dose rate of 65 Gy min^{-1} ± 3.1% was determined. At the center of the 7.62 cm (3 inch) diameter canister with no canister present, a dose rate of 37 Gy min^{-1} ± 3.1% was measured. These values are much closer to the quoted 45 Gy min^{-1} dose rate. The dose rate to tissue in thin-shelled oysters was 14.1 Gy min^{-1} ± 6.5%, and the dose rate to tissue in thick-shelled oysters was about 15% less than that at 12.3 Gy min^{-1} ± 6.5%.

Table 6. Absorbed dose and dose equivalent rates to shelled and unshelled tissue at various voltages. All doses are given at the maximum allowable current settings in 10.2 cm (4 inch) diameter corrugated plastic canister.

	Dose rate to tissue, no shell				Dose rate to tissue in thin oyster shell				Dose rate to tissue in thick oyster shell			
kV	Exposure rate (R min^{-1})	Dose rate (Gy min^{-1}) (Sv min^{-1})	Dose rate (rad min^{-1}) (rem min^{-1})	% error	Exposure rate (R min^{-1})	Dose rate (Gy min^{-1}) (Sv min^{-1})	Dose rate (rad min^{-1}) (rem min^{-1})	% error	Exposure rate (R min^{-1})	Dose rate (Gy min^{-1}) (Sv min^{-1})	Dose rate (rad min^{-1}) (rem min^{-1})	% error
30	0.18	0.00	0.17	30.6%[a]	*measurements not taken for shelled oyster phantoms at grayed voltages*							
40	1.91	0.02	1.82	3.6%								
50	6.90	0.07	6.56	3.1%								
60	23.09	0.22	21.94	2.8%								
70	53.54	0.51	50.87	2.8%								
80	105.36	1.00	100.10	3.2%								
90	181.85	1.73	172.76	2.9%								
100	284.23	2.70	270.02	2.8%	302.46	2.87	287.34	2.9%	266.25	2.53	252.94	3.1%
110	419.52	3.99	398.56	3.2%	455.54	4.33	432.77	2.8%	395.04	3.75	375.30	2.8%
120	606.96	5.77	576.63	2.8%	637.94	6.06	606.05	3.2%	547.84	5.20	520.45	3.1%
125	747.17	7.10	709.82	2.8%								
130	910.07	8.65	864.58	2.8%	929.96	8.83	883.48	2.8%	799.39	7.59	759.43	2.8%
135	1064.40	10.11	1011.20	2.8%								
140	1256.23	11.93	1193.44	2.8%	1084.17	10.30	1029.98	2.8%	933.79	8.87	887.12	2.8%
145	1459.48	13.87	1386.53	2.8%								
150	2099.24	19.94	1994.32	4.1%	1485.89	14.12	1411.62	3.4%	1298.02	12.33	1233.14	3.1%

[a] the large error is due to the fact that the reading uncertainty is a large percent of the exposure measurement.

Dose to Plants and Seeds

Faculty members at Mississippi State University have indicated an interest in irradiating plants and seeds to induce mutations. While the dose necessary to induce mutations depends on the plant type, an acute dose on the order of 500 Gy is adequate for many species. In his textbook, van Harten (1998) gives examples of mutations induced from doses in the range of 100 to 350 Gy for peas, 300 to 450 Gy for barley, and 450 to 600 Gy for tomatoes. At the maximum operating parameters, the RS 2400 can deliver doses of these magnitudes in well under one hour.

The elemental composition, and therefore Z_{eff} value, also varies greatly by plant type. For example, Z_{eff} of dry onion seeds was calculated to be 6.62 while Z_{eff} of begonia seeds was 18.9 (Table 7) (Zhang et al. 2002; West and Lott 1991). Seeds typically have much lower water content than tissue, particularly if they have been dried for storage, so dose to tissue is not a good approximation of the dose to seeds (Robinson 1975).

Table 7. Z_{eff} for dry onion and begonia seeds.

Element	Z	Weight percent	
		Dry onion seeds	Begonia seeds
calcium	20	0.31%	12% ± 8%
carbon	6	51.70%	—
chlorine	17	0.08%	—
hydrogen	1	7.61%	—
iron	26	0.01% [a]	—
magnesium	12	0.33%	32% ± 2%
nitrogen	7	4.15%	—
oxygen	8	33.40%	—
phosphorus	15	0.61%	—
potassium	19	0.73%	48% ± 1%
silicon	14	0.02%	—
sulfur	16	0.79%	22% ± 5%
Z_{eff} =		6.62	18.9

[a] elements less than 0.01% by weight are not listed (total adds to 99.74%) (Zhang et al. 2002)
[b] determined by neutron activation analysis (West and Lott 1991)

Because Mississippi State University does not yet know what species of plant or kind of tissue it will irradiate, no attempt was made to calculate a particular Z_{eff} value or find the corresponding μ_{en}/ρ value. Rather, it is suggested that they use the method outlined by Dasberg (1971) to determine the attenuation coefficient, μ. While not identical to μ_{en}, it is a suitable approximation. A detector capable of measuring radiation intensity (in units of radiation events, exposure, absorbed dose, or dose equivalent), a radiation source (preferably of identical energy and type of radiation to be used in irradiation), and the type of seeds or plant material to be irradiated are required. The detector placed in the field of radiation and the unattenuated radiation intensity, I_0,

should be measured. Without changing the source and detector geometry, a layer of seeds should be placed between the two. The seeds should completely cover the radiation field so that only radiation passing through the seeds reaches the detector. The intensity of radiation should be measured again, but this is the attenuated intensity, *I*. The attenuation is described by eqn (15)

$$I = I_0\, e^{-\mu t} \tag{15}$$

where *t* is the thickness of the seed layer (typically given in cm) and μ is in cm^{-1}. For example, the detector could be placed on the floor of the RS 2400 with an empty container, in which the seeds will later be placed, on top of the detector face. The seed container should completely cover the sensitive area of the detector face. The first measurement, I_0, could be taken with the irradiator operating at the current and voltage that will be used in irradiation. The seeds or plant material can be added to the container and the second measurement, *I*, taken. Using eqns (13), (15) and the density of the seeds, the dose to seed can be determined.

During irradiation, the seeds or plant material can be placed in a thin, low *Z* container, such as a paper envelope or plastic bag, without worry of reducing the x-ray dose. A quick comparison showed no significant differences in exposure rates between a bare FIC and a FIC covered with a plastic bag at either 60 kV or 150 kV (and the maximum current settings). However, all irradiations should be done with as little material surrounding the sample as possible, as thick husks or packaging can reduce the number of x rays that reach the sample.

CHAPTER IV

SUMMARY AND CONCLUSIONS

The RS 2400 delivers exposure as expected over its operating range of 30 kV to 150 kV and 2 mA to 45 mA. As expected, the exposure rate increased as the current and voltage are increased. With the exception of the first 5 cm (2 inches) on the left of the x-ray tube, the x-ray beam exposure is uniform within 10% across a wide range of operating voltages. Support structures in the first 5 cm greatly reduce the x-ray beam. To ensure uniform exposure, samples to be irradiated should not be placed in the first 2.5 cm (1 inch) on the left of the canister. At the maximum operating values of 150 kV and 45 mA, the beam was uniform within 3.1%.

Oyster shells reduced the exposure to oyster tissue, most significantly when the voltage was greater than 130 kV. At the highest operating parameters (150 kV and 45 mA), thick oyster shells reduced the unshelled exposure rate by approximately 38% and thin oyster shells reduced the exposure rate by approximately 29%. There was consistently a 15% ± 4.6% difference between the thick-shelled and thin-shelled exposure rates. If the experimenter is able to classify the oysters as generally thick-shelled or generally thin-shelled, he should use the exposure and dose rate values associated with that shell. If the experimenter cannot generally classify the shell thickness, the average value between the two should be used adding 7.5% to the uncertainty in the exposure rate or dose rate.

At maximum operating parameters (150 kV and 45 mA) on the surface of the x-ray tube with no canister, a dose rate of 65 Gy min^{-1} ± 3.1% was measured. At the center of the 7.62 cm (3 inch) diameter canister with no canister present, a dose rate of 37 Gy min^{-1} ± 3.1% was determined. These values are similar to the 45 Gy min^{-1} dose rate given by Rad Source Technologies, Inc. (2007b).

For irradiation, oysters will most likely be placed in the 10.2 cm (4 inch) diameter plastic canister since the 7.62 cm (3 inch) diameter canisters are not wide enough to hold larger oysters. The oyster shells and increased distance from the x-ray source reduced the maximum deliverable dose rate. The maximum deliverable dose rate to thin-shelled oysters was 14.1 Gy min^{-1} ± 6.5%. While impressively high for an x-ray irradiator, a 1 kGy exposure to these oysters would still take about seventy minutes. The thick-shelled oysters would take 14% longer, or about 80 minutes, to receive the same dose. The ESPL will need to determine if this is an acceptable amount of time to remove the oysters from the tanks. If it is not, perhaps they should experiment with cooling the oysters during irradiation or delivering the dose in fractions.

REFERENCES

Andrews LS, Ahmedna M, Grodner RM, Liuzzo JA, Murano PS, Murano EA, Rao RM, Shane S, Wilson PW. Food preservation using ionizing radiation. Rev Environ Contam Toxicol 154:1–53; 1998.

Attix FH. Introduction to radiological physics and radiation dosimetry. Berlin, Germany: Wiley-VCH; 2004.

Bomford CK, Kunkler IH, Walter J. Walter and Miller's textbook of radiotherapy: radiation physics, therapy, and oncology. 6th ed. New York: Churchill Livingstone; 2002. Available at: http://books.google.com/books?id=YBYNJvsmpxsC. Accessed 1 March 2008.

Dasberg S. Soil water movement to germinating seeds. J Exp Bot 22:999–1008; 1971.

Dinwiddie SC, Yadock W, Johnson DO, Tretter C, Redmond W, Nelson KA. X-ray radiation as an alternative to gamma radiation for irradiation of blood components. Transfusion 40 Supplement:157S–158S; 2000.

Engineers Edge. Properties of metals. Available at: http://www.engineersedge.com/properties_of_metals.htm. Accessed 1 May 2008.

Federline MV. NRC promulgation of the energy policy act of 2005. Volume 71, Number 7, Federal Register, January 11, 2006. Available at: http://www.radsource.com/pdf/nrc.pdf. Accessed 19 May 2008.

Feldman LC, Mayer JW. Fundamentals of surface and thin film analysis. Amsterdam: Prentice Hall PTR; 1986.

Hendrichs J. To our readers. Insect Pest Control Newsletter 68:1–2; 2007.

Hu X, Mallikarjunan P, Koo J, Andrews LS, Jahncke ML. Comparison of kinetic models to describe high pressure and gamma irradiation used to inactivate *Vibrio vulnificus* and *Vibrio parahaemolyticus* prepared in buffer solution and in whole oysters. J Food Protect 68:292–295; 2005.

Jakabi M, Gelli DS, Torre JCMD, Rodas MAB, Franco BDGM, Destro MT, Landgraf M. Inactivation by ionizing radiation of *Salmonella enteriditis*, *Salmonella infantis*, and *Vibrio parahaemolyticus* in oysters *(Crassostrea brasiliana*). J Food Protect 66:1025–1029; 2002.

Jayachandran CA. Calculated effective atomic number and kerma values fro tissue-equivalent and dosimetry materials. Phys Med Biol 16:617–623; 1971.

Johns HE, Cunningham JR. The physics of radiology. 4th ed. Springfield, IL: Charles C Thomas; 1983.

Johnston WR. Database of radiological incidents and related events: Johnston's archive. Available at: http://www.johnstonsarchive.net/nuclear/radevents/index.html. Accessed 25 September 2007.

Kirkup L. Data analysis with Excel: an introduction for physical scientists. New York: Cambridge University Press; 2002. Available at: http://books.google.com/books?id=rDsec-JnCAwC. Accessed 1 March 2008.

Knoll GF. Radiation detection and measurement. 3rd ed. Ann Arbor, MI: John Wiley & Sons, Inc.; 2000.

Krippl, E. The International Atomic Energy Agency's laboratories: Seibersdorf and Vienna, meeting the challenges of research and international co-operation in the application of nuclear techniques. Vienna: IAEA Division of Public Information; 1996.

Mehta K. Gamma radiation vs. x-radiation. Available at: http://radsource.com/gammaVx-rays.html, 2007. Accessed 8 October 2007.

Nuclear Enterprises Limited. 2571 specifications bulletin No 132. Reading, England: Nuclear Enterprises Limited; 1980.

Rad Source Technologies, Inc. Technical proposal for a high output canister irradiator RS 2500. Prepared for the IAEA. Alpharetta, GA: Rad Source Technologies; 2007a.

Rad Source Technologies, Inc. RS 2400 operations and maintenance manual. Alpharetta, GA: Rad Source Technologies; 2007b.

Robertson CB, Andrews LS, Marshall DL, Coggins P, Schilling MW, Martin RE, Collette R. Effect of x-ray irradiation on reducing the risk of listeriosis in ready-to-eat vacuum-packaged smoked mullet. J Food Protect 69**:**1561–1564; 2006.

Robinson AS. Genetic basis of the SIT. In: Dyck VA, Hendrichs J, Robinson AS, eds. Sterile insect technique: principles and practice in area-wide integrated pest management. Dordrecht, The Netherlands: Springer; 2005.

Robinson RG. Amino acid and elemental composition of sunflower and pumpkin seeds. Agron J 67:541–544; 1975.

Rugh R, Wolff J. X-irradiation sterilization of the female mouse. Fertility and Sterility 7:546–560; 1956.

Texas A&M University Nuclear Science Center. X-ray operating procedures and calibrations manual. College Station: Texas A&M University Nuclear Science Center; 2001.

U.S. Nuclear Regulatory Commission (NRC). Requirement for advance notice and protection of import shipments of nuclear material from countries that are not party to the convention on the physical protection of nuclear material. Washington, DC: U.S. Government Printing Office; 10 CFR Part 73.74; 2008. Available at: http://www.nrc.gov/reading-rm/doc-collections/cfr/part073/part073-0074.html. Accessed 1 December 2007a.

U.S. Nuclear Regulatory Commission (NRC). Units of radiation dose. Washington, DC: U.S. Government Printing Office; 10 CFR Part 20.1004; 2002. Available at: http://www.nrc.gov/reading-rm/doc-collections/cfr/part020/part020-1004.html. Accessed 1 December 2007b.

Van Harten AM. Mutation breeding: theory and practical applications. New York: Cambridge University Press; 1998.

Winter M. Web elements periodic table. Available at http://webelements.com/. Accessed 1 May 2008.

West MM, Lott JNA. A histological and elemental analysis study of the mature seed of *Begonia semperflorens*. Can J Bot 69:2165—2169; 1991.

Zhang W, Endo S, Ishikawa M, Ikeda H, Hoshi M. Relative biological effectiveness of fission neutrons for producing micronuclei in the root-tip cells of onion seedlings after irradiation as dry seeds. J Radiat Res 43:397–403; 2002.

Supplemental Sources Consulted

Hall EJ, Giaccia AJ. Radiobiology for the radiologist. 6th ed. Philadelphia: Lippincott Williams & Wilkins; 2006.

Liu C, Chen R, Su Y. Bactericidal effects of wine on *Vibrio parahaemolyticus* in oysters. J Food Protect 69:1823–1828; 2006.

Mississippi Department of Health. Regulations for control of radiation in Mississippi. Title 15, Part III, Subpart 78. http://www.msdh.state.ms.us/msdhsite/ _static/resources/ 1708.pdf. Accessed 8 Jan 2008.

Tamhane AC, Dunlop DD. Statistics and data analysis from elementary to intermediate. Upper Saddle River, NJ: Prentice Hall; 2000.

Turner JE. Atoms, radiation, and radiation protection. 2nd ed. New York: John Wiley & Sons, Inc.; 1995.

APPENDIX A

Preliminary Calibration of Farmer-type Ion Chambers. Measurements taken at 250 kV, 10.0 mA.

FIC 1			FIC 2		
NSC FIC (R)	FIC 1 (R)	Calibration Factor (Ratio NSC/FIC 1)	NSC FIC (R)	FIC 2 (R)	Calibration Factor (Ratio NSC/FIC 2)
46.18	45.4	1.02	89.50	67.55	1.32
125	127	0.98	80.94	60.60	1.34
84.6	86.4	0.98	74.18	55.38	1.34
64.59	65.46	0.99			
65.56	68.58	0.96[a]			
43.13	*misread*	*n/a*	*Only 3 measurements taken for FIC 2 calibration*		
43.94	*73.22*	*0.60*			
45.55	*73.18*	*0.62*[b]			
73.92	74.24	1.00			
70.18	68.54	1.02			
	AVERAGE	**0.99 ± 0.9%**			**1.33 ± 0.5%**

[a] adjusted shelf on which ion chambers were sitting after this measurement

[b] adjusted ion chambers after this measurement and the ratio returned to ~1. I believe that the NSC FIC was out of the x-ray beam. The grayed values are excluded from the average calibration factor.

APPENDIX B

Calibration of Farmer-type Ion Chamber 2. All measurements taken at 9.0 mA.

kV	Disk Ion Chamber (counts)	*s* (R)	NSC FIC (R)	*s* (R)	FIC 2 (R)	Calibration Factor (Ratio NSC/FIC 2)
100	30869	175.70	50.05	0.78	34.33	1.46
	30247	173.92	49.00	0.78	33.78	1.45
	30328	174.15	48.66	0.78	33.79	1.44
						avg (100 kV) = 1.45
125	60687	246.35	93.46	0.88	65.91	1.42
	60877	246.73	92.93	0.88	65.85	1.41
	90803	301.34	93.50	0.81	65.64	1.42
						avg (125 kV) = 1.42
150	60265	245.49	91.87	0.87	63.54	1.45
	67086	259.01	95.80	0.87	70.60	1.36
	65253	255.45	92.51	0.86	68.43	1.35
	64209	253.39	91.71	0.86	66.77	1.37
						avg (150 kV) = 1.38
			Average Calibration Factor (all kV) =			**1.42 ± 2.78%**

APPENDIX C

Exposure rate as a function of linear position.

kV	mA	Position (inches from left)	Exposure rate (R min^{-1})	% error (R min^{-1})	Average exposure rate (R min^{-1}), pos. 2-9	% difference from pos. 2-9 average
60	6.8	0	22.70	3.25%		72.99%
		1	48.45	2.90%		42.37%
		2	77.56	3.04%		7.75%
		3	81.49	2.80%		3.07%
		4	80.51	2.81%		4.23%
		5	82.09	3.33%		2.36%
		6	76.46	2.80%		9.05%
		7	91.69	2.77%		9.07%
		8	91.27	2.89%		8.56%
		9	91.48	2.86%	84.07	8.82%
120	20.3	0	681.22	3.08%		66.96%
		1	1316.24	2.83%		36.16%
		2	1950.51	3.09%		5.39%
		3	2090.80	2.99%		1.41%
		4	2022.08	2.78%		1.92%
		5	2024.63	2.95%		1.80%
		6	1959.03	2.94%		4.98%
		7	2185.95	2.77%		6.03%
		8	2141.64	2.81%		3.88%
		9	2118.64	2.93%	2061.66	2.76%
150	45	0	1349.00	4.90%		65.53%
		1	2520.86	4.28%		35.58%
		2	3550.71	2.78%		9.27%
		3	3997.48	4.79%		2.15%
		4	3979.91	2.87%		1.70%
		5	3853.17	3.51%		1.54%
		6	3851.57	2.78%		1.58%
		7	4134.86	3.78%		5.66%
		8	3933.05	2.92%		0.51%
		9	4005.47	2.94%	3913.28	2.36%

APPENDIX D

Exposure rate and dose rate to tissue at surface of x-ray tube, centered along the length of the tube. Maximum allowable current setting for voltage was used.

kV	Exposure rate ($R\ min^{-1}$)	Dose rate ($Gy\ min^{-1}$) ($Sv\ min^{-1}$)	Dose rate ($rad\ min^{-1}$) ($rem\ min^{-1}$)	% error
30	0.00	0	0	0.00%
40	11.08	0.11	11	7.60%
50	29.51	0.28	28	4.78%
60	97.31	0.92	92	3.60%
70	252.76	2.4	240	3.29%
80	452.98	4.3	430	3.20%
90	785.26	7.46	746	3.15%
100	1251.02	11.88	1188	3.13%
110	1808.23	17.18	1718	3.15%
120	2565.66	24.37	2437	3.13%
125	3026.73	28.75	2875	3.14%
130	3632.08	34.51	3451	3.13%
140	4722.92	44.87	4487	3.13%
145	4722.92	44.87	4487	3.13%
150	6876.35	65.33	6533	3.13%

Exposure rate and dose rate to tissue at center of 7.62 cm (3 inch) diameter cardboard canister, centered along the length of the tube. Maximum allowable current setting for voltage was used.

kV	Exposure rate ($R\ min^{-1}$)	Dose rate ($Gy\ min^{-1}$) ($Sv\ min^{-1}$)	Dose rate ($rad\ min^{-1}$) ($rem\ min^{-1}$)	% error
30	0.31	0.00	0.30	59.1% [a]
40	3.69	0.04	3.51	10.09%
50	14.26	0.14	13.54	6.29%
60	44.91	0.43	42.67	5.89%
70	104.57	0.99	99.34	5.89%
80	209.45	1.99	198.98	5.89%
90	358.02	3.40	340.13	5.89%
100	571.12	5.43	542.58	5.89%
110	841.47	7.99	799.41	5.89%
120	1177.25	11.18	1118.41	5.89%
125	1411.48	13.41	1340.93	5.89%
130	1705.7	16.20	1620.45	5.89%
135	2028.9	19.27	1927.49	5.89%
140	2243.74	21.32	2131.59	5.89%
145	2602.86	24.73	2472.76	5.89%
150	3698.96	35.14	3514.08	5.89%

[a] the large error is due to the fact that the reading uncertainty is a large percent of the exposure measurement.

Exposure rate and dose rate to tissue at center of 7.62 cm (3 inch) diameter aluminum canister, centered along the length of the tube. Maximum allowable current setting for voltage was used.

kV	Exposure rate ($R\ min^{-1}$)	Dose rate ($Gy\ min^{-1}$) ($Sv\ min^{-1}$)	Dose rate ($rad\ min^{-1}$) ($rem\ min^{-1}$)	% error
30	0.13	0.00	0.12	141.1% [a]
40	1.73	0.02	1.65	13.69%
50	7.98	0.08	7.58	7.19%
60	27.85	0.26	26.45	6.19%
70	67.86	0.64	64.47	6.09%
80	143.99	1.37	136.79	5.89%
90	250.68	2.38	238.15	5.89%
100	410.88	3.90	390.34	5.89%
110	618.41	5.88	587.50	5.89%
120	897.87	8.53	852.99	5.89%
125	1111.15	10.56	1055.61	5.89%
130	1321.24	12.55	1255.20	5.89%
135	1585.57	15.06	1506.32	5.89%
140	1826.12	17.35	1734.85	5.89%
145	1975.79	18.77	1877.03	5.89%
150	2857.61	27.15	2714.78	5.89%

[a] the large error is due to the fact that the reading uncertainty is a large percent of the exposure measurement.

VITA

Name: Jennifer Koop Wagner

Address: Jennifer Koop Wagner
Department of Nuclear Engineering
Texas A&M University 3133
College Station, TX 77843-3133

Email Address: jenkoop@gmail.com

Education: B.S., Radiological Health Engineering, Texas A&M University, 2005
M.S., Health Physics, Texas A&M University, 2008